

Geothermal heating enhances atmospheric asymmetries on synchronously rotating planets

Jacob Haqq-Misra^{1,2,*} and Ravi Kumar Kopparapu^{1,2,3,4,5}

¹Blue Marble Space Institute of Science, 1200 Westlake Ave N Suite 1006, Seattle, WA 98109, USA

²Virtual Planetary Laboratory, PO Box 351580, Seattle, WA 98195, USA

³Department of Geosciences, Pennsylvania State University, 443 Deike Building, University Park, PA 16802 USA

⁴Center for Exoplanets & Habitable Worlds, Pennsylvania State University, 525 Davey Lab, University Park, PA 16802 USA

⁵Penn State Astrobiology Research Center, Pennsylvania State University, 2217 Earth and Engineering Sciences Building, University Park, PA 16802 USA

This version 2014 July 4

ABSTRACT

Earth-like planets within the liquid water habitable zone of M type stars may evolve into synchronous rotators. On these planets, the sub-stellar hemisphere experiences perpetual daylight while the opposing anti-stellar hemisphere experiences perpetual darkness. Because the night-side hemisphere has no direct source of energy, the air over this side of the planet is prone to freeze out and deposit on the surface, which could result in atmospheric collapse. However, general circulation models (GCMs) have shown that atmospheric dynamics can counteract this problem and provide sufficient energy transport to the anti-stellar side.

Here we use an idealized GCM to consider the impact of geothermal heating on the habitability of synchronously rotating planets. Geothermal heating may be expected due to tidal interactions with the host star, and the effects of geothermal heating provide additional habitable surface area and may help to induce melting of ice on the anti-stellar hemisphere. We also explore the persistence of atmospheric asymmetries between the northern and southern hemispheres, and we find that the direction of the meridional circulation (for rapidly rotating planets) or the direction of zonal wind (for slowly rotating planets) reverses on either side of the sub-stellar point. We show that the zonal circulation approaches a theoretical state similar to a Walker circulation only for slowly rotating planets, while rapidly rotating planets show a zonal circulation with the opposite direction. We find that a cross-polar circulation is present in all cases and provides an additional mechanism of mass and energy transport from the sub-stellar to anti-stellar point. Characterization of the atmospheres of synchronously rotating planets should include consideration of hemispheric differences in meridional circulation and examination of transport due to cross-polar flow.

Key words: planets and satellites: terrestrial planets – stars: low-mass – planets and satellites: atmospheres – hydrodynamics – astrobiology.

1 INTRODUCTION

Low-mass M stars are among the most numerous stellar type in the galaxy and also among the most long lived. This would make them attractive candidates in the search for life beyond Earth were it not for the possibility of atmospheric loss due to synchronous rotation. The ongoing discovery of extrasolar planets around low-mass stars (Basri et al. 2005; Udry et al. 2007; Von Bloh et al. 2008; Bonfils et al. 2013; Anglada-Escudé et al. 2013) has renewed discussion of the habitability of planets orbiting M type stars (Tarter et al. 2007) and provides additional motivation for understanding the atmospheric dynamics of such planets.

The observation of extrasolar planets around stars of all

types has increased interest in characterizing planetary atmospheres through climate modeling. These include general circulation model (GCM) simulations of atmospheric circulation on large, Jupiter-sized planets in close orbit to their parent star known as “hot Jupiters” (Cooper & Showman 2005; Fortney et al. 2006; Showman et al. 2008; Menou & Rauscher 2009; Showman & Polvani 2011), as well as consideration of smaller, Neptune-sized gas giants and Earth-sized terrestrial planets (Williams & Holloway 1982; Heng et al. 2011). The discovery of planets orbiting the M type star Gliese 581 also prompted an assessment of the habitability of these new worlds that include radiative climate calculations of Gliese 581c (Hu & Ding 2011). (Note that radiative and GCM studies also were conducted for the suspected planets Gliese 581d (von Paris et al. 2010; Hu & Ding 2011) and Gliese 581g (Heng & Vogt 2011; Pierrehumbert 2011), which have now been determined to be ar-

* E-mail: jacob@bmsis.org

tifacts due to stellar activity (Robertson et al. 2014.) These modeling studies help to identify prominent circulation features in the atmospheres of extrasolar planets and characterize the types of atmospheres that could exist in orbit around distant stars

One way to characterize planetary habitability is the liquid water habitable zone (Kasting et al. 1993; Kopparapu et al. 2013, 2014), which describes the region around a star where a planet could sustain surface liquid water. This habitable zone defines a region where the negative climate feedback of the carbonate-silicate cycle (Walker et al. 1981) can keep a planet above freezing. It is bounded on the inner edge by the loss of water through initiation of a runaway greenhouse effect (Kasting 1988) and on the outer edge by the condensation of carbon dioxide (Kasting 1991). Although this habitable zone cannot be generalized to all extrasolar planets, it can be used to characterize the habitability of any terrestrial planet with water and a carbonate-silicate cycle. (Some authors have extended consideration of habitability to scenarios such as a dry planet with limited water (Abe et al. 2011; Zsom et al. 2013) or a planet rich in atmospheric hydrogen (Pierrehumbert & Gaidos 2011).) For low-mass M type stars, this liquid water habitable zone falls within the tidal locking orbital distance of its parent star, so any potentially habitable planets around these stars (according to this definition of habitability) are at risk of atmospheric loss and may in fact be uninhabitable.

The problem of atmospheric stability for planets orbiting low-mass stars has been investigated by Joshi et al. (1997), Joshi (2003), Merlis & Schneider (2010), Edson et al. (2011), Pierrehumbert (2011), Heng & Vogt (2011), Selsis et al. (2011), Edson et al. (2012) Yang et al. (2013), Leconte et al. (2013), and Yang et al. (2014) using GCMs to assess the degree to which atmospheric circulations can maintain planetary habitability. These simulations show that a range of planetary atmospheres can remain stable under synchronous rotation, either by a sufficiently dense carbon dioxide atmosphere (Joshi et al. 1997; Joshi 2003; Selsis et al. 2011; Edson et al. 2012) or in regimes where atmospheric dynamics provides sufficient heat transport to the night side (Merlis & Schneider 2010; Edson et al. 2011; Pierrehumbert 2011; Heng & Vogt 2011). These GCM studies demonstrate that extrasolar planets orbiting low-mass stars can indeed provide habitable conditions at locations on the surface, even with the problem of synchronous rotation.

In this study we use an idealized GCM to investigate the influence of geothermal heating on atmospheric dynamics. We present a set of experiments that include fast and slow rotators to show that geothermal heating amplifies asymmetries in atmospheric circulation between the northern and southern hemispheres, which can cause transient regions of warming near the anti-stellar point. We show that the dynamical structure of the atmosphere changes on either side of the sub-stellar point, and we find that a cross-polar circulation provides transport from the day to night side in all experiments. These results provide qualitative descriptions of the expected meridional, zonal, and cross-polar circulation patterns that can help to guide further GCM studies of synchronously rotating planets.

2 SYNCHRONOUS ORBITS AROUND LOW-MASS STARS

A planet can fall into synchronous rotation around its parent star when tidal dissipation slows down the planet's rotation rate. Not all planets orbiting at this tidal locking distance from the parent star will necessarily become synchronous rotators, such as those

with eccentric orbits or with close neighbors so that they fall into spin-orbit resonances. For example, the planet Mercury is within the tidal locking distance of our sun, but it has fallen into a 3:2 spin-orbit resonance that remains stable because of its nonzero eccentricity. Planets with more circular orbits, however, may evolve into synchronous rotators so that a single side is fixed at perpetual daylight, while the opposing side experiences perpetual night.

The tidal migration history of any particular planet depends on factors such as the initial rate of rotation, eccentricity, and semi-major axis (Jackson et al. 2008a,b,c; Barnes et al. 2009), which complicates efforts to determine a particular orbital distance at which a planet should be expected to fall into a synchronously rotating state. No single analytic equation can describe the tidal locking radius for all planetary systems, and empirical formulae may be limited in their predictive power. In this section we use such an empirical equation to demonstrate limits on stellar mass and rotation rate for these systems; however, we admit that this approach is simplistic and neglects many key factors that contribute to the actual tidal history of a planetary system.

The tidal locking distance r_T can be described empirically (Peale 1977; Kasting et al. 1993; Dobrovolskis 2009; Edson et al. 2011) according to the formula

$$r_T = 0.024 \left(\frac{P_0 t}{Q} \right)^{1/6} M^{1/3}, \quad (1)$$

where M is the mass of the parent star, P_0 is the original rotation period of the planet, t is the time period since planetary formation, and Q is a parameter describing the inverse of the specific dissipation function for the entire planet. We restrict our focus in this study to synchronously rotating Earth-like planets, which allows us to specify the parameters in Eq. (1). We assume early Earth rotated more rapidly than today so that $P_0 = 13.5$ hr (Walker & Zahnle 1986; Kasting et al. 1993; Williams 2000; Edson et al. 2011), and we likewise use the 4.5 billion year formation period of Earth as the value of t . The parameter Q has a relatively low value on Earth today (~ 13) because most tidal dissipation occurs from gravitational interactions with the sun and Moon along oceanic shorelines (Kasting et al. 1993). However, this present-day value may be unusually large (Kasting et al. 1993; Edson et al. 2011), and different continental configurations on early Earth—such as a larger ocean (Rosing et al. 2010)—could have reduced the tidal dissipation rate. We will therefore use a value of $Q = 100$ as characteristic of early Earth (Burns 1986; Kasting et al. 1993; Edson et al. 2011) to describe tidal forces on a synchronously rotating Earth-like planet. The value of the tidal locking distance r_T in Eq. (1) is only weakly sensitive to changes in the parameters P_0 , t , and Q , so the primary contributor is the mass M of stellar types that could induce synchronous rotation for orbiting Earth-like planets.

We consider an Earth-like planet to be a terrestrial planet that receives the same incident flux of stellar radiation as Earth. The stellar flux F reaching a planet at an orbital radius r is related to the luminosity of its star L according to $F = L/(4\pi r^2)$. We can examine planets in orbit around different stellar types by defining the Earth equivalent distance of a planet r_{EED} as the orbital distance at which a planet receives an equal magnitude of radiation from its parent star as Earth does from the sun (Edson et al. 2011). At the Earth equivalent distance, the flux equals that on Earth, so we can write

$$\frac{L}{L_{\odot}} = \left(\frac{r_{EED}}{r_{\oplus}} \right)^2, \quad (2)$$

where L_{\odot} is the luminosity of the sun, and r_{\oplus} is the orbital radius of Earth. If we use the general approximation that stellar luminosity for low-mass stars is proportional to mass to the fourth power $L \sim M^4$, then we can combine Eqs. (1) and (2) by setting $r_T \leq r_{EED}$ and solving for stellar mass. Letting M_{\odot} be the mass of the sun, we find that

$$\frac{M}{M_{\odot}} \leq \left[0.024 \left(\frac{P_{0t}}{Q} \right)^{1/6} \frac{M_{\odot}^{1/3}}{r_{\oplus}} \right]^{3/5}. \quad (3)$$

Substituting in values for the parameters in Eq. (3) shows that the Earth equivalent distance r_{EED} and the tidal locking distance r_T intersect at $M/M_{\odot} \approx 0.6$; planets in orbit around stars less massive than this will be in synchronous rotation at the Earth equivalent distance. This means that F, G, and K type stars are unlikely to harbor Earth-like planets in synchronous rotation, but smaller M type stars are ideal candidates to find such planets.

We use this mass limit to calculate the maximum rotation rate for a synchronously rotating Earth-like planet. Kepler’s third law gives the relation $(r_{EED}/r_{\oplus})^3 (M_{\odot}/M) = (P_{EED}/P_{\oplus})^2$, where P_{EED} and P_{\oplus} are the orbital period at the Earth equivalent distance and at Earth’s present distance, respectively. This corresponds to an upper limit on orbital period (equivalently, rotation rate) of $P_{EED} \approx 230$ days for synchronously rotating Earth-like planets around M type stars (c.f. Edson et al. (2011)). Planets rotating faster than this limit may still be prone to synchronous rotation, while planets rotating slower than this limit will be beyond the tidal locking distance and outside the liquid water habitable zone (Kopparapu et al. 2013, 2014). In this study, we consider synchronously rotating planets with both 1-day (“fast”) and 230-day (“slow”) rotation rates to show the similarities and differences that arise in these two dynamical regimes.

3 GENERAL CIRCULATION MODEL

We use a general circulation model (GCM) to simulate the atmospheres of synchronously rotating Earth-like planets and investigate the influence of geothermal heating. This GCM uses a hydrostatic spectral dynamical core (with T42 resolution), two-stream gray radiative transfer, a diffusive boundary layer scheme, and a surface slab ocean (Frierson et al. 2006; Haqq-Misra et al. 2011). We set obliquity to zero and adjust the incoming solar radiation profile so the sub-stellar point is fixed on the intersection of the equator (0° latitude) and international date line (180° longitude). We also include a geothermal heat flux in the GCM by adding a constant term to the surface temperature tendency equation.

This model is still highly idealized, as the model atmosphere is transparent to incoming stellar radiation and absorbs only infrared radiation emitted upward from the surface. Water vapor is assumed to be radiatively neutral, so this GCM does not include any water vapor feedback, and the model experiments also do not include any topography or cloud formation. Although some of these processes will likely be significant in determining specific features of climate, these idealizations help to highlight large-scale dynamical patterns and make the model an ideal tool for investigating the prominent circulation patterns that arise on synchronously rotating planets.

We consider both dry and moist regimes for our GCM experiments. We force dry GCM conditions by setting the saturation vapor pressure equal to zero and using dry adiabatic adjustment. The moist regime includes latent heat release through large-scale condensation, and a simplified shallow penetrative adjustment also known as Betts-Miller adjustment (Frierson 2007). For non-synchronously rotating Earth-like planets, the presence of moisture in this GCM acts to increase static stability and reduce circulation strength (Haqq-Misra et al. 2011). These idealized dry and moist configurations are designed to emphasize the key differences in atmospheric dynamics that arise from the presence or absence of water vapor.

We conduct a series of GCM experiments using fast (1-day) and slow (230-day) rotation rates with 25 vertical levels and physical properties identical to those used by Haqq-Misra et al. (2011). We initialize dry and moist control states at each rotation rate with a constant temperature at all grid points and run the GCM for a 3000 day spin-up period to reach a statistically steady state. Geothermal heating is then enabled (or kept disabled), and the model is allowed to continue adjusting for another 500 days. We then use the subsequent 1000 days of model output in the analysis that follows. Running this GCM using a Linux workstation (6-core Intel E5-2620 Xeon 2.0 GHz) requires approximately 8 hours in real-time to calculate 1000 model days.

Table 1 lists the eight GCM experiments we consider in this study. We use the designators “fast” and “slow” in reference to 1-day and 230-day rotation periods, respectively, and we likewise indicate “dry” and “moist” cases accordingly. We use “control” to refer to experiments without any geothermal flux, and “geothermal” indicates the presence of a 2.0 W m^{-2} geothermal heat flux across the entire surface. This set of eight GCM experiments provide an overview of expected large-scale dynamical structures and the resulting perturbations that arise from geothermal heating.

4 GEOTHERMAL HEATING

Terrestrial planets in synchronous rotation around low-mass stars experience tidal heating from gravitational interactions with the host star (Jackson et al. 2008a,b,c; Barnes et al. 2009; Heller & Barnes 2013; Barnes et al. 2013). Within the Solar System, Io exhibits strong tidal interactions as it orbits Jupiter, which drives constant volcanism across the moon’s surface. This form of tidal heating also should occur for extrasolar planets in synchronous rotation (Jackson et al. 2008a; Barnes et al. 2009, 2013) and even for some exomoons (Heller & Barnes 2013). The magnitude of tidal heating for any particular planet depends on its orbital geometry and tidal migration history (Jackson et al. 2008b,c), but some degree of tidal heating should be expected to arise on most synchronously rotating planets.

We consider the effects of tidal heating in the GCM as a geothermal heat flux applied uniformly across all surface grid points. Actual profiles of tidal heating on synchronously rotating planets likely will show latitudinal and longitudinal variations, but we choose this idealized representation as a first-order estimation of the influence of a geothermal heat flux. We choose a value of 2.0 W m^{-2} for the geothermal heat flux in our model, which approximately corresponds to the tidal heat flux on Io (Heller & Barnes 2013). We do not represent any additional internal heat fluxes, such as from radiogenic decay, so these calculations can be considered as an upper limit on the influence of tidal heating on surface temperature and atmospheric circulation.

Table 1. A list of GCM experiments conducted for this study.

Experiment Name	Rotation Rate	Convective Adjustment	Hydrologic Cycle	Geothermal Heating
Fast Dry Control	1 day	dry adiabatic	none	-
Fast Dry Geothermal	1 day	dry adiabatic	none	2.0 W m ⁻²
Fast Moist Control	1 day	shallow Betts-Miller	large-scale condensation	-
Fast Moist Geothermal	1 day	shallow Betts-Miller	large-scale condensation	2.0 W m ⁻²
Slow Dry Control	230 days	dry adiabatic	none	-
Slow Dry Geothermal	230 days	dry adiabatic	none	2.0 W m ⁻²
Slow Moist Control	230 days	shallow Betts-Miller	large-scale condensation	-
Slow Moist Geothermal	230 days	shallow Betts-Miller	large-scale condensation	2.0 W m ⁻²

Our GCM experiments include control cases (no geothermal heat flux) and geothermal cases (2.0 W m⁻² geothermal heat flux) run under dry and moist conditions at both fast and slow rotation rates (Table 1). Fig. 1 shows the time average of surface temperature and horizontal wind \bar{u}, \bar{v} for the full set of experiments. Note that here and elsewhere we show surface temperature as the deviation from the freezing point of water. The top row of Fig. 1 shows the control cases, the middle row shows the geothermal cases, and the bottom row shows the difference between the geothermal and control cases. Note that each panel is centered on the anti-stellar point (at 0° latitude and 0° longitude) to emphasize the changes in temperature and wind that occur across the anti-stellar hemisphere. A noticeable shift in wind patterns occurs between fast and slow rotators, which is an expected regime transition (Merlis & Schneider 2010; Edson et al. 2011; Yang et al. 2014; Leconte et al. 2013) that will be discussed further in Section 5. Asymmetries also persist between the northern and southern hemisphere in all cases, which has been noted by others (Merlis & Schneider 2010; Yang et al. 2013, 2014) and also will be discussed further in Section 5. The presence of geothermal heating (Fig. 1, bottom row) provides warming across the surface as expected; however, the distribution of warming yields regions near the anti-stellar point with asymmetric warm or cold features between the northern and southern hemispheres that persist even after averaging over 1000 days. These effects are most pronounced in the fast dry cases, with deviations of ± 5 K and asymmetric wind patterns around the anti-stellar point. The presence of moisture appears to reduce the asymmetric influence of geothermal heating, although some asymmetric features between the northern and southern hemispheres still persist. The slow rotators show the most uniform effect from geothermal heating, with only slight asymmetries in the time average of surface temperature and horizontal wind.

The asymmetric features between the northern and southern hemispheres observed in the time average quantities shown in Fig. 1 are the result of transient variations in atmospheric dynamics across the anti-stellar hemisphere. The transient evolution of surface temperature and horizontal wind difference (geothermal minus control) is shown in Fig. 2 at 100-day intervals for the full set of experiments. (Animations of transient evolution for all GCM experiments are available online.) In all cases, geothermal heating shows stronger regions of warming and cooling that are asymmetrically distributed between the northern and southern hemispheres near the anti-stellar point and fluctuate with time. The fast dry case shows the strongest deviations of ± 20 K or more, while the presence of moisture reduces these changes by about a factor of two. Asymmetric features are also prominent in the slow dry case, with surface temperature changes of about ± 5 K or so and slight reductions in the corresponding fast moist case. These experiments all suggest that geothermal heating acts to create or amplify asymmet-

ric circulation features between the northern and southern hemispheres that cause transient regions of warming and cooling most prominent near the anti-stellar point.

Geothermal heating enhances the persistence of asymmetric features by affecting the formation of large-scale dynamical structures responsible for energy transport. Even in a dry atmosphere, strong thermally-direct circulations (discussed further in Section 5) are sensitive to changes in the surface energy flux, which alters the transport of mass and energy from the sub-stellar to anti-stellar point and generates a slightly different pattern in the general circulation. The net effect is that the added energy from uniform geothermal heating is distributed unevenly across the surface through dynamical energy transport, which allows some additional cycles of warming and cooling to persist between the northern and southern hemispheres near the anti-stellar point.

Even without geothermal heating, asymmetric features between the northern and southern hemispheres have been observed in other GCM simulations (Merlis & Schneider 2010; Yang et al. 2013, 2014) and appear to be a robust phenomenon of synchronous rotation. We even attempted to initialize the GCM into a fully symmetric synchronously rotating state without any baroclinic eddies (following the approach of Haqq-Misra et al. (2011) for non-synchronous rotation), but the model immediately lost its symmetry and reverted to the states presented here. These asymmetric features seem to persist regardless of the averaging period or sampling variability and do not appear sensitive to other changes in the model configuration. These results all suggest that the asymmetric features seen in GCMs are not artifacts of averaging but are dynamically-induced features of the atmosphere that affect the distribution of surface temperature between the northern and southern hemispheres, particularly near the anti-stellar point.

5 ATMOSPHERIC CIRCULATION

The atmospheric circulation on synchronously rotating planets is known to exhibit unique three-dimensional behavior that is markedly different from the prominent circulations on Earth, such as equatorial superrotation and heat transport from the anti-stellar to sub-stellar point (Joshi et al. 1997; Joshi 2003; Merlis & Schneider 2010; Edson et al. 2011; Showman & Polvani 2011). Some of this behavior is captured by typical meridional and zonal mass streamfunctions, but we show below that careful consideration of the wind field is required to accurately describe the most prominent means of transport.

We describe the mean meridional circulation (MMC) with a mass streamfunction Ψ_M that calculates the northward mass flux

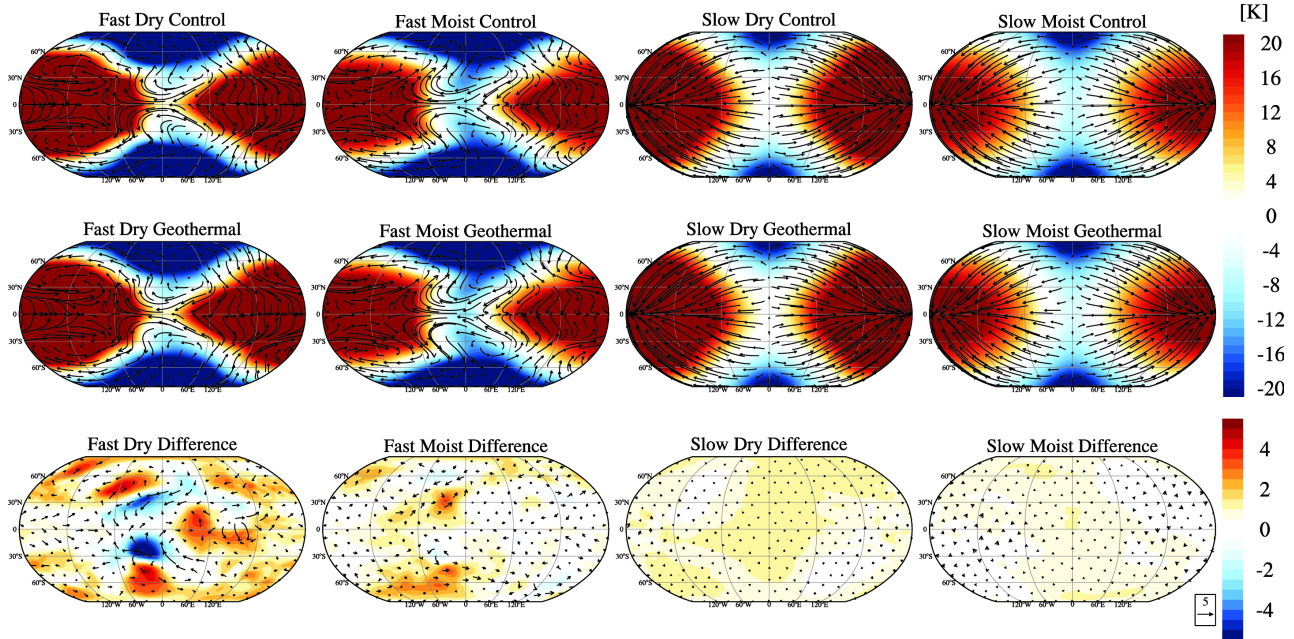


Figure 1. Time average of surface temperature deviation from the freezing point of water (shading) and horizontal wind \bar{u}, \bar{v} (vectors) for a synchronously rotating planet for the (first column) fast dry, (second column) fast moist, (third column) slow dry, and (fourth column) slow moist experiments. The top row shows control cases with no geothermal flux, the middle row shows geothermal cases with a 2.0 W m^{-2} geothermal flux, and the bottom row shows the difference between geothermal and control cases. The sub-stellar point is centered on the equator along the international date line, and each panel is centered on the anti-stellar point (0° latitude and longitude).

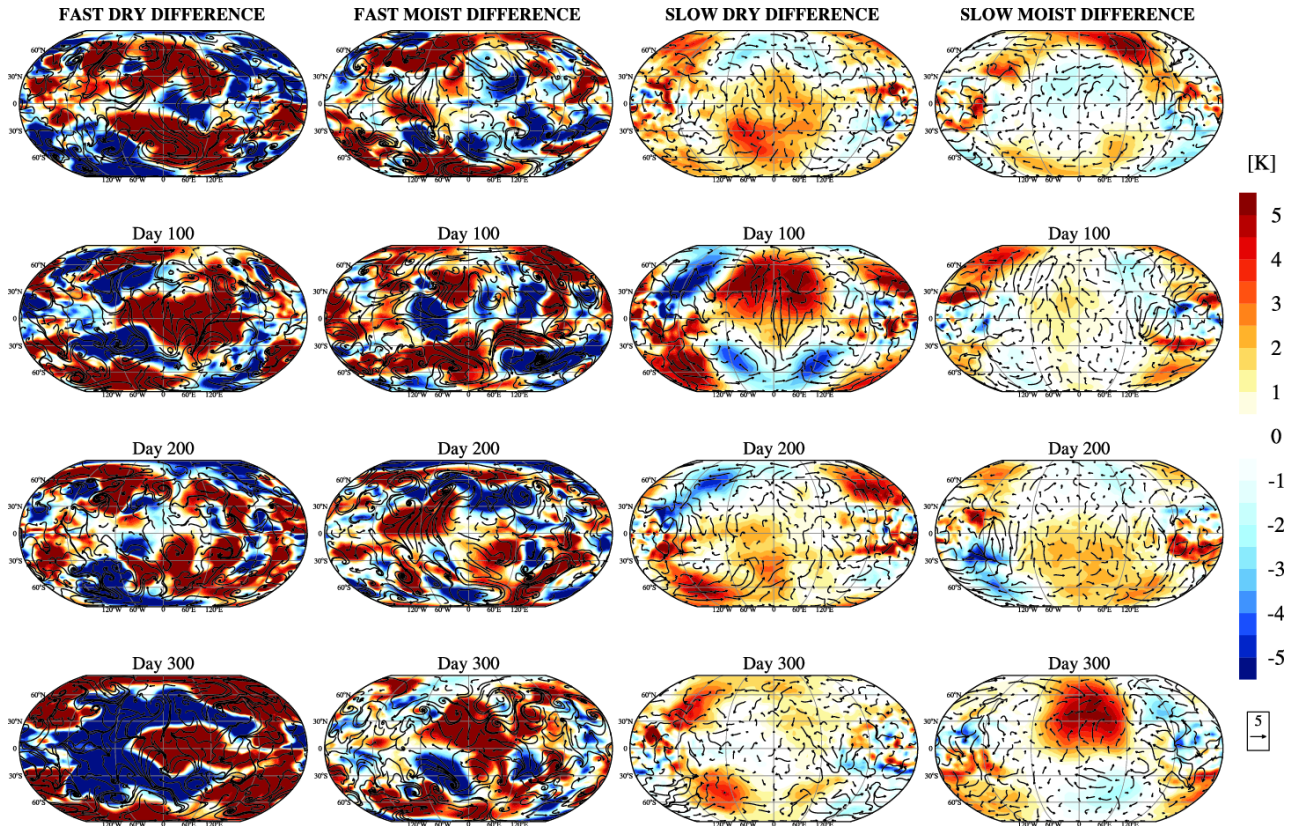


Figure 2. Transient evolution of the surface temperature deviation from the freezing point of water (shading) and horizontal wind u, v (vectors) difference between the geothermal and control cases for the (first column) fast dry, (second column) fast moist, (third column) slow dry, and (fourth column) slow moist experiments. Each row shows instantaneous conditions at intervals of 100 days. (Animations of these experiments are available online.)

above a particular pressure level p' as

$$\Psi_M = \frac{2\pi a \cos \phi}{g} \int_0^{p'} \bar{v} dp. \quad (4)$$

This streamfunction traces out the familiar patterns of the MMC when applied to Earth models or time-averaged observations, showing direct (i.e., Hadley) and indirect (i.e., Ferrel) circulation cells. On Earth, and other planets not in synchronous rotation, the MMC is a primary driver of meridional heat transport from the tropics to poles and results in the formation of a subtropical jet and polar front jet along the edge of the circulation cells Frierson et al. (2006).

For planets in synchronous rotation, the MMC still acts as a means of meridional heat transport, but the geometry of the circulation depends strongly upon rotation rate. Fig. 3 shows the MMC Ψ_M and zonal mean zonal wind \bar{u} for the full set of experiments. The fast rotators all show similar patterns of a Hadley, Ferrel, and polar cell similar to Earth, but the upper atmosphere features strong superrotation in a single eastward equatorial jet with westward flow only at the very top of the model. The slow rotators show an entirely different MMC configuration, with direct cells elevated above the surface and indirect cells circulating from equator to pole. The zonal wind for the slow rotators appears to be zero, which we show below results from a change in circulation across hemispheres. Note that the difference between geothermal and control cases (Fig. 3, bottom row) results in asymmetric structures that are weak in strength but emphasize the role of geothermal heating in creating small asymmetries in circulation between the northern and southern hemispheres. The strength of the MMC is also stronger in dry cases compared to their moist counterparts, which occurs because the presence of water vapor increases static stability and decreases the magnitude of overturning circulations (Haqq-Misra et al. 2011).

The MMC shown in Fig. 3 can be misleading, however, as the circulation pattern changes depending on position relative to the sub-stellar point. This observation was made by Geisler (1981) in application to a simplified model of the Walker circulation, where it was noticed that the direction of the MMC changes on either side of the heating source. On Earth, the Walker circulation is a transient phenomenon, but on synchronously rotating planets the star shines fixed on a single location at all times, so this theoretical prediction may be even more relevant. We therefore may expect that the patterns of circulation in our GCM experiments should change between the hemispheres east and west of the sub-stellar point.

Fig. 4 shows the MMC Ψ_M and zonal mean zonal wind \bar{u} separated over the eastern hemisphere and western hemisphere from the sub-stellar point for the set control of experiments. The fast rotators all show a change in direction of the MMC, with the eastern hemisphere showing circulation in the same direction as in Fig. 3 and the western hemisphere showing circulation in the opposite direction. The atmosphere is still superrotating for the fast rotators, although the equatorial jet is much stronger in the eastern hemisphere, and notable differences persist between hemispheres in the geometry of the MMC cells. By contrast, the slow rotators do not show a change in circulation direction, but instead the wind direction changes from eastward in the eastern hemisphere to westward in the western hemisphere. Slight asymmetries are apparent in the MMC between the northern and southern hemispheres, but the slow rotators appear to maintain a relatively consistent geometry across the sub-stellar point. The contrast between the zonally averaged quantities in Fig. 3 and the hemispheric separation made in Fig. 4 provides one example of the circulation features that contribute to persistent atmospheric asymmetries.

The zonal circulation, also known as the Walker circulation, provides another possible mechanism for transporting energy from the sub-stellar to anti-stellar point. On Earth, the Walker circulation is characterized by rising motion at the heating source, eastward (and westward) flow aloft as air descends, and return flow along the surface back toward the heating source (Gill 1980; Geisler 1981). We describe the mean zonal circulation (MZC) with a mass streamfunction Ψ_Z that calculates the eastward mass flux above a particular pressure level p' as

$$\Psi_Z = \frac{2\pi a}{g} \int_0^{p'} \bar{u}^* dp, \quad (5)$$

where \bar{u}^* is the zonal average value minus the time-average component of zonal wind. The extent of this circulation is limited by the propagation of equatorially trapped Rossby waves and equatorial Kelvin waves (Gill 1980; Showman & Polvani 2011), which provides an explanation for the regime transition in wind patterns observed between fast and slow rotators in Fig. 1. Edson et al. (2011) describes a change in patterns of winds that occurs when the Rossby deformation radius (which is inversely proportional to rotation rate) begins to approach the planetary radius at a rotation rate of about 4.2 days. This regime shift has also been noted by others (Merlis & Schneider 2010) and is evident in many different GCMs (Yang et al. 2014; Leconte et al. 2013). At least for the slow rotators, we expect that the zonal circulation should provide a circulation that reaches from the sub-stellar to the anti-stellar point.

Fig. 5 shows the MZC Ψ_Z and vertical wind $-\bar{w}$ for the full set of experiments. The slow rotators do indeed show a characteristic Walker-like circulation with rising motion at the sub-stellar point, eastward (and westward) motion aloft, sinking motion near the sub-stellar point, and return flow along the surface. The fast rotators show the opposite sense: sinking motion in the vicinity near the sub-stellar point, and rising motion within the anti-stellar hemisphere. Because the Rossby deformation radius is small compared to the planetary radius, the MZC cells for the fast rotators span a shorter longitudinal extent and does not fully reach the anti-stellar point. Conversely, the slow rotators have a larger Rossby deformation radius that allows the MZC to traverse a full hemisphere. Geothermal heating appears to have relatively negligible effects on the MZC in all cases, while variations in vertical wind due to geothermal heating appear only in the fast rotators.

The MMC and MZC provide a partial description of the circulation on synchronously rotating planets, but the three-dimensional features noted by others (Joshi et al. 1997; Joshi 2003; Edson et al. 2011) include a cross-polar circulation that appears in all our GCM experiments and acts as an additional means of transport from the sub-stellar to anti-stellar point. Fig. 6 shows a polar stereographic plot of eddy heat flux $v'\theta'$ and horizontal wind for the set of fast rotators, where θ is potential temperature and the primes denote deviations from the zonal mean. Following Joshi et al. (1997), the zonal mean also has been removed from all zonal wind vectors. The first and third columns of Fig. 6 show the 950 hPa surface just above the ground, while the second and fourth columns show the 150 hPa surface at the top of the troposphere. In both dry and moist cases, a cross-polar circulation is evident with flow from the anti-stellar point to sub-stellar point along the surface, rising motion at the heating source, and flow aloft from the sub-stellar point back across the pole to the anti-stellar point. Likewise, Fig. 7 shows a polar stereographic plot of eddy heat flux and horizontal wind for the set of slow rotators, which shows the same cross-polar circulation pattern with more pronounced patterns of superrotation. Geothermal heating helps to increase the magnitude of superrotation in all

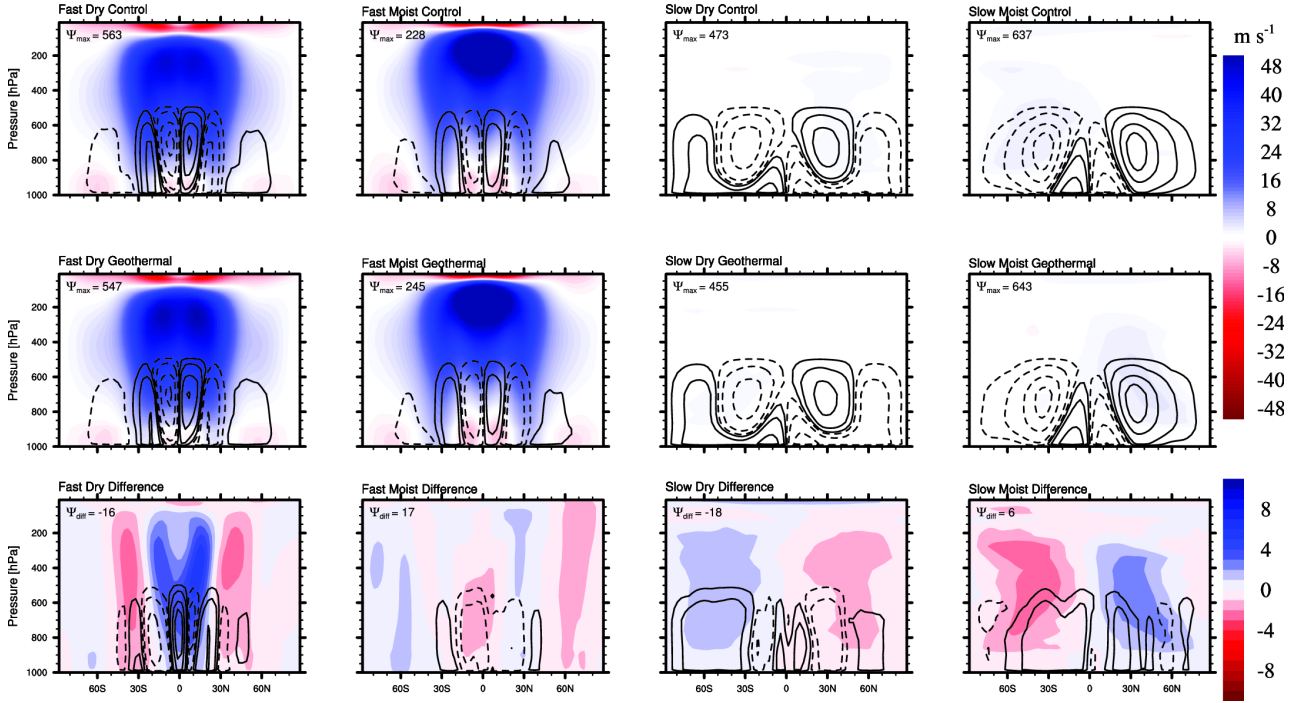


Figure 3. Mean meridional circulation Ψ_M (line contours) and zonal mean zonal wind \bar{u} (shading) for the (first column) fast dry, (second column) fast moist, (third column) slow dry, and (fourth column) slow moist experiments. The top row shows control cases, the middle row shows geothermal cases, and the bottom row shows the difference between geothermal and control cases. Contours are drawn at an interval of $\pm\{20, 100, 300, 500, 700, 1000\} \times 10^9 \text{ kg s}^{-1}$ for the top two rows and at $\pm\{5, 20, 60, 100\} \times 10^9$ for the bottom row. The maximum streamfunction Ψ_{max} is shown on each panel in units of 10^9 kg s^{-1} . Solid contours indicate clockwise circulation, and dashed contours indicate counter-clockwise circulation.

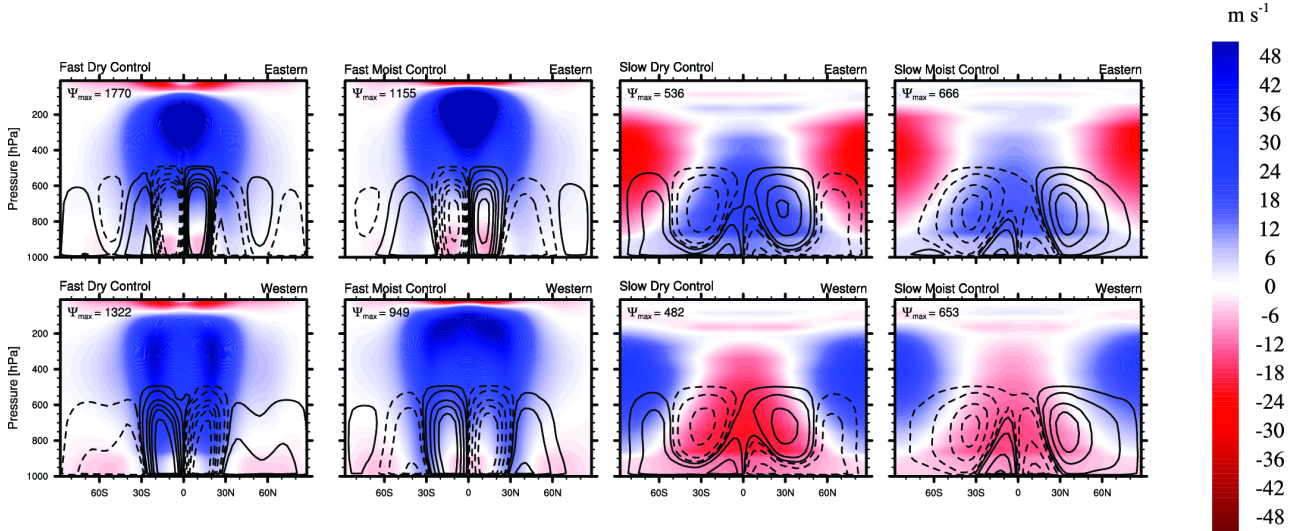


Figure 4. Mean meridional circulation Ψ_M (line contours) and zonal mean zonal wind \bar{u} (shading) averaged across the (top row) eastern hemisphere and (bottom row) western hemisphere from the sub-stellar point for the (first column) fast dry, (second column) fast moist, (third column) slow dry, and (fourth column) slow moist control experiments. Contours are drawn at an interval of $\pm\{20, 100, 300, 500, 700, 1000\} \times 10^9 \text{ kg s}^{-1}$, and the maximum streamfunction Ψ_{max} is shown on each panel in units of 10^9 kg s^{-1} . Solid contours indicate clockwise circulation, and dashed contours indicate counter-clockwise circulation.

these experiments, which increases the transport of mass and energy to the anti-stellar point by enhancing the cross-polar flow.

The cross-polar circulation appears to be evident as a means of transport from the sub-stellar to anti-stellar point in all these experiments. The MMC and MZC also provide prominent circulations that maintain transient asymmetries between the northern and southern hemispheres, although only in the slow rotators where the

Rossby deformation radius is large does the MZC also contribute to this transport. Fig. 8 shows a schematic diagram of the cross-polar circulation that contributes to energy transport on synchronously rotating planets. This polar flow is present in all our experiments, regardless of rotation rate or geothermal heating, and should be a robust circulation feature in the atmospheres of synchronously rotating Earth-like planets.

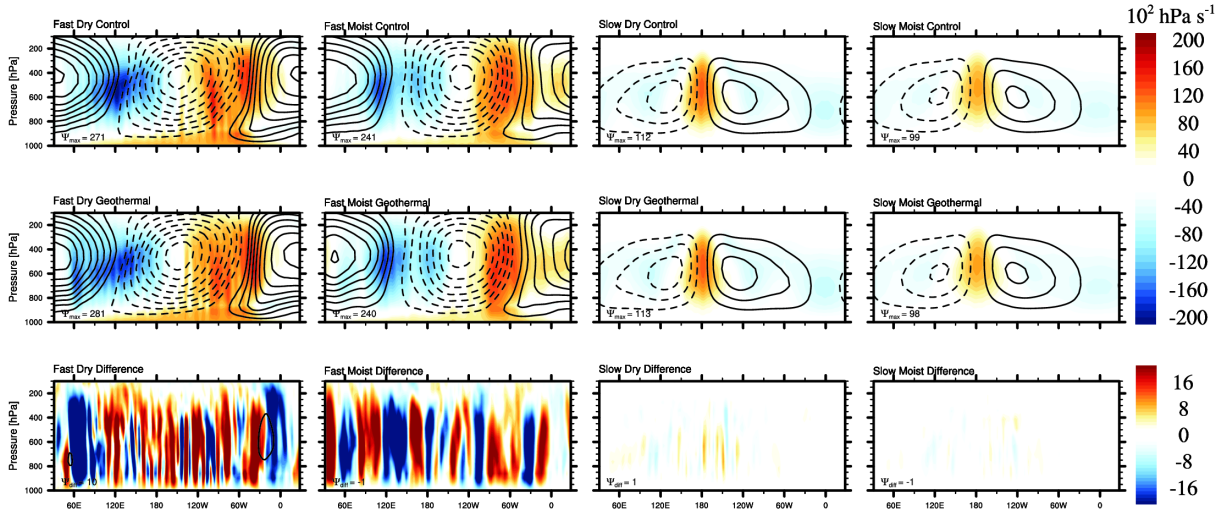


Figure 5. Mean zonal circulation Ψ_Z (line contours) and vertical wind $-\bar{w}$ (shading) for the (first column) fast dry, (second column) fast moist, (third column) slow dry, and (fourth column) slow moist experiments. The contour interval for the mean zonal circulation is $30 \times 10^{11} \text{ kg s}^{-1}$ for the fast rotators and $30 \times 10^{13} \text{ kg s}^{-1}$ for the slow rotators, and the maximum streamfunction Ψ_{max} is shown on each panel in units of $10^{11} \text{ kg s}^{-1}$ and $10^{13} \text{ kg s}^{-1}$, respectively. Solid contours indicate clockwise circulation, and dashed contours indicate counter-clockwise circulation. Zonal wind speeds have been reduced in the slow rotator cases by a factor of 10.

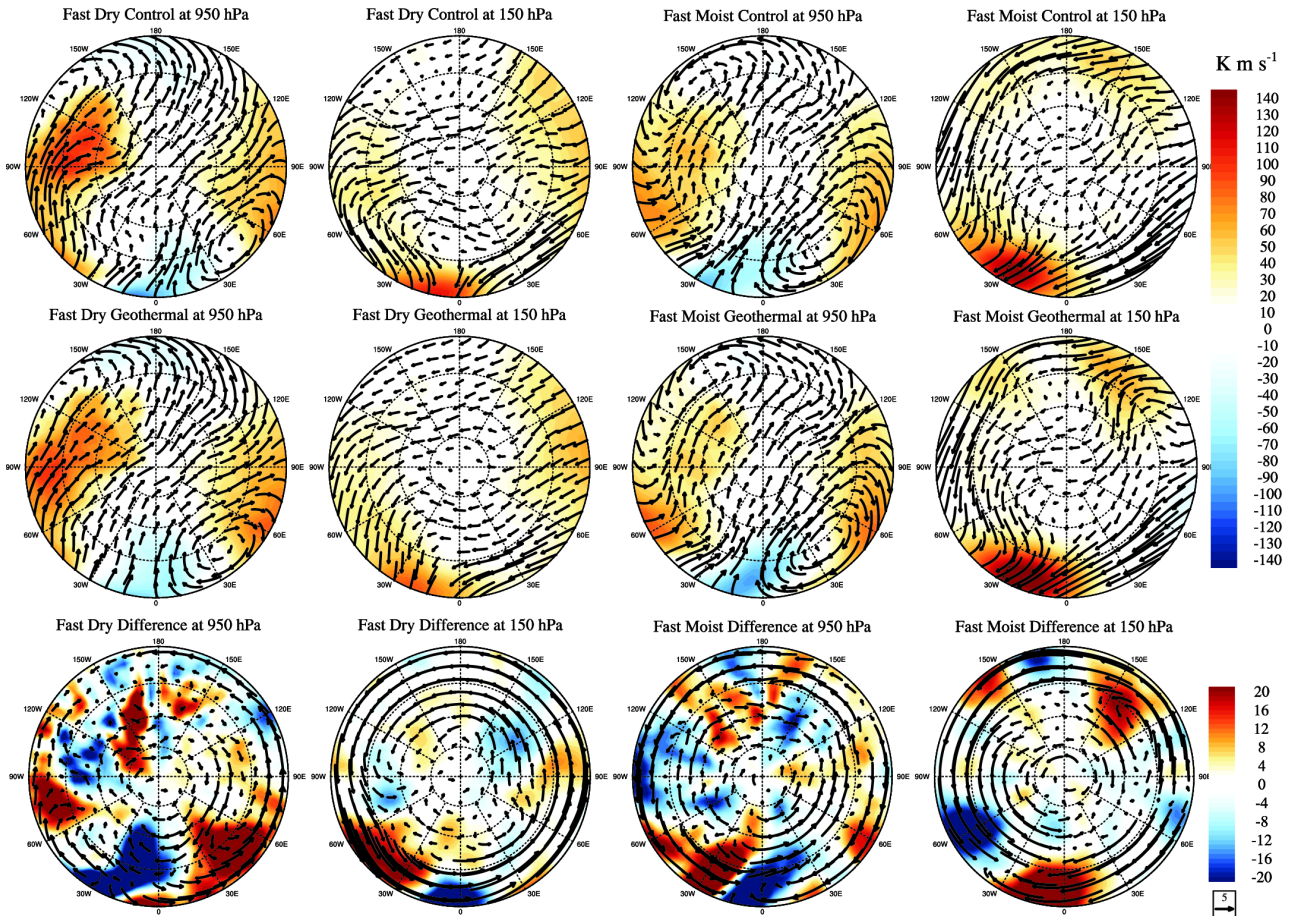


Figure 6. Polar stereographic plots of eddy heat flux $\overline{v'\theta'}$ (shading) and horizontal wind \bar{u}, \bar{v} (vectors) on the (first and third columns) 950 hPa surface and (second and fourth columns) 150 hPa surface for the (first and second columns) fast dry and (third and fourth columns) fast moist experiments. The top row shows control cases, the middle row shows geothermal cases, and the bottom row shows the difference between geothermal and control cases. The plot shows the northern hemisphere from 30° to 90° latitude, and the zonal mean is removed from all zonal wind vectors.

namical patterns. The cross-polar circulation on slow rotators complements the zonal circulation so that surface winds everywhere are drawn into the sub-stellar point and carried aloft toward the anti-stellar point.

In general, the presence of the cross-polar circulation provides an additional mechanism for transporting energy and mass from the sub-stellar to anti-stellar point. Linearized theory based on the analysis of the Walker circulation on Earth suggests analogous structures for the circulation on synchronous rotators (Gill 1980; Geisler 1981; Showman & Polvani 2011), but these theoretical expectations of a zonal circulation reaching from the sub-stellar to anti-stellar point only seem to apply to slow rotators where the Rossby deformation radius is large. Faster rotators, with a smaller Rossby deformation radius, do not exhibit significant zonal transport, but the pattern of the cross-polar circulation perhaps is more consistent with theory. This suggests that any GCM simulations (and, someday, observations) of synchronously rotating planets should consider the mass transport by the cross-polar circulation, rather than the meridional or zonal circulations exclusively, as a means of characterizing the dynamics of climate.

The climate of a synchronously rotating planet is sometimes described using the term “eyeball Earth” to denote open water beneath the sub-stellar point, relatively clement conditions along the surface in a surrounding ring, and ice-covered conditions everywhere else all the way to the anti-stellar hemisphere (Pierrehumbert 2011; Angerhausen et al. 2013). If geothermal heating can cause regions of transient warming through the enhancement of large-scale circulations, then regions of melting could create cratered pockets of ice, slowly flowing glaciers, or even standing liquid water around the anti-stellar point. This suggests that “eyeball Earth” planets might include a soft spot on the side farthest from the heat source. Further investigation with GCM’s coupled to ice sheet models will help to constrain the range of climates on which this could occur.

7 CONCLUSIONS

Low mass M-type stars provide some of the closest and most numerous targets for current exoplanet surveys, and the discovery of synchronously rotating planets within the habitable zones of these stars will increase interest in the atmospheric characterization of such worlds. We have considered a set of experiments that include slow rotators (1 day) toward the inner edge of the habitable zone and fast rotators (230 days) toward the outer edge of the habitable zone. Between these fast and slow rotators is a regime transition where superrotation dominates, but the general patterns discussed from this limited set of experiments should extend appropriately to other rotation rates within the habitable zone.

Tidal heating can produce a geothermal heat flux that warms the surface of a synchronously rotating planet, which can cause transient regions of warming and cooling of up to ± 20 K or more on the anti-stellar hemisphere. This enhanced warming could contribute to increased ice melt along the anti-stellar point and extend the habitable surface area of the planet. This effect is stronger on fast rotators, and the presence of moisture also tends to reduce the magnitude of anomalous regions. The presence of geothermal heating acts to enhance asymmetries between the northern and southern hemispheres that alter the structure of large-scale circulation features such as the MMC, the MZC, and the cross-polar circulation.

The dynamics of synchronous rotators include different patterns on either side of the sub-stellar point. The fast rotators exhibit a change in the direction of the Hadley circulation from the eastern

to western hemisphere, while the slow rotators show a change in the direction of zonal wind. The Walker circulation provides transport of mass and energy from the sub-stellar to anti-stellar point only for slow rotators, while fast rotators show a Walker circulation with the opposite sense. In all cases, a cross-polar circulation provides an additional mechanism for transport of mass and energy from the sub-stellar to anti-stellar point. Fast rotators maintain asymmetric features such as large-scale jets and vortices at mid-latitudes, while slow rotators have transitioned to a superrotation regime, but all experiments show a cross-polar circulation that provides or enhances the transport from day side to night side. Typical considerations of the Hadley and Walker circulation therefore may be insufficient for synchronously rotating planets, with the cross-polar circulation and hemispheric meridional circulation providing more accurate descriptions of atmospheric transport.

Our set of experiments is designed to highlight important features in the large-scale dynamics of synchronously rotating planets. The idealized GCM used in this study cannot provide precise orbital limits to habitability, but the simplified nature of this model allows the most fundamental atmospheric processes to be more apparent. More accurate representation of clouds and radiative transfer will improve the model’s ability to predict particular climates for specific planetary configurations, but the general patterns of large-scale dynamics should remain consistent across the parameter space described here. As astronomers continue the hunt for alien worlds and turn their eyes to low mass stars nearby, atmospheric modelers should continue the quest to understand circulation patterns on worlds very much unlike our own.

ACKNOWLEDGMENTS

Funding for this research was provided by the NASA Astrobiology Institute’s Virtual Planetary Laboratory under awards NNX11AC95G,S03 (J.H.) and NNH05ZDA001C (R.K.K.).

REFERENCES

- Abe Y., Abe-Ouchi A., Sleep N.H., Zahnle K.J., 2011, *Astrobiology*, 11, 443
- Angerhausen D., et al., 2013, *Astrobiology*, 13, 309
- Anglada-Escudé G., et al., 2013, *A&A*, 556, A126
- Barnes R., Jackson B., Greenburg R., Raymond S.N., 2009, *ApJ*, 700, L30
- Barnes R., Mullins K., Goldblatt C., Meadows V.S., Kasting J.F., Heller R., 2013, *Astrobiology*, 13, 225
- Basri G., Borucki W. Kock D., 2005, *New Astron Rev*, 49, 478
- Bonfils X., et al., 2013, *A&A*, 556, A110
- Burns J.A., 1986, *Satellites*, University of Arizona, Tuscon, p. 117
- Cooper C.S., Showman A.P., 2005, *ApJ*, 629, L45
- Dobrovolskis A.R., 2009, *Icarus*, 204, 1
- Dole S.H., 1964, *Habitable Planets for Man*, Blaisdell, New York
- Edson A.R., Lee S., Bannon P.R., Kasting J.F., Pollard D., 2011, *Icarus*, 212, 1
- Edson A.R., Kasting J.F., Pollard D., Lee S., Bannon P.R., 2012, *Astrobiology*, 12, 562
- Fortney J.J., Cooper C.S., Showman A.P., Marley M.S., Freedman R.S., 2006, *ApJ*, 652, 746
- Frierson D.M.W., Held I.M., Zurita-Gotor P., 2006, *J Atmos Sci*, 63, 2548
- Frierson D.M.W., 2007, *J Atmos Sci*, 64, 1959

- Geisler J.E., 1981, *J Atmos Sci*, 38, 1390
 Gill A.E., 1980, *Quar J R Met Soc*, 106, 447
 Haqq-Misra J., Lee S., Frierson D.M.W., 2011, *J Atmos Sci*, 68, 2930
 Heller R., Barnes R., 2013, *Astrobiology*, 13, 18
 Heng K., Menou K., Phillipps P.J., 2011, *MNRAS*, 413, 2380
 Heng K., Vogt S.S., 2011, *MNRAS*, 415, 2145
 Hu Y., Ding F., 2011, *A&A*, 526, A135
 Jackson B., Barnes R., Greenberg R., 2008, *MNRAS*, 391, 237
 Jackson B., Greenberg R., Barnes R., 2008, *ApJ*, 678, 1396
 Jackson B., Greenberg R., Barnes R., 2008, *ApJ*, 681, 1631
 Joshi M., Haberle R.M., Reynolds R.T., 1997, *Icarus*, 129, 450
 Joshi M., 2003, *Astrobiology*, 3, 415
 Kasting J.F. 1988, *Icarus*, 74, 472
 Kasting J.F. 1991, *Icarus*, 94, 1
 Kasting J.F., Whitmire D.P., Reynolds R.T., 1993, *Icarus*, 101, 108
 Kopparapu R.K., et al., 2013, *ApJ*, 765, 131
 Kopparapu R.K., Ramirez R.M., SchottelKotte J., Kasting J.F., Domagal-Goldman S., Eymet V., 2014, *ApJ*, 787, L29
 Leconte J., et al., 2013, *A&A*, 554, A69
 Menou K., Rauscher E., 2009, *ApJ*, 700, 887
 Merlis T.M., Schneider T., 2010, *JAMES*, 2, 13
 Peale S.J., 1977, *Planetary Satellites*, University of Arizona, Tucson, p. 87
 Pierrehumbert R.T., 2011, *ApJ*, 726, L8
 Pierrehumbert R.T., Gaidos E.J., 2011, *ApJ*, 734, L13
 Robertson P., Mahadevan S., Endl M., Roy A., 2014, *Science*, doi:10.1126/science.1253253
 Rosing M.T., Bird D.M., Sleep N.H., 2010, *Nature*, 464, 744
 Selsis F., Wordsworth R., Forget F., 2011, *A&A*, 532, A1
 Showman A.P., Cooper C.S., Fortney J.J., Marley M.S., 2008, *ApJ*, 652, 746
 Showman A.P., Polvani L.M., 2011, *ApJ*, 738, 1
 Tarter J.C., et al., 2007, *Astrobiology*, 7, 30
 Udry S., et al., 2007, *A&A*, 469, 43
 Von Bloh W., Bounama C., Cuntz M., Franck S., 2008, *A&A*, 33, 275
 von Paris P., 2010, *A&A*, 522, A23
 Walker J.C.G., Hays P.B., Kasting J.F., 1981, *J Geophys Res*, 86, 9776
 Walker J.C.G., Zahnle K.J., 1986, *Nature*, 320, 600
 Williams G.P., Holloway J.L., 1982, *Nature*, 297, 295
 Williams G.E., 2000, *Rev Geophys*, 38, 39
 Yang J., Cowan N.B., Abbot D.S., 2013, *ApJ*, 771, L45
 Yang J., Boué G., Fabrycky D.C., Abbot D.S. 2014, *ApJ*, 787, L2
 Zsom A., Seager S., de Wit J., Stamenković V., 2013, *ApJ*, 778, 109